ACS APPLIED MATERIALS & INTERFACES

Research Article

Cite This: ACS Appl. Mater. Interfaces 2018, 10, 36369−36376

www.acsami.org

Microtubes with Complex Cross Section Fabricated by C-Shaped Bessel Laser Beam for Mimicking Stomata That Opens and Closes Rapidly

Deng Pan,[†,‡] Ze Cai,[†,‡] Shengyun Ji,[†,‡] Shengying Fan,[†,‡] Pengrui Wang,[§,∥] Zhaoxin Lao,[†,‡] Liang Yang,[†,‡] Jincheng Ni,[†,‡] Chaowei Wang,[†,‡] Jiawen Li,*[†,‡] Yanlei Hu,[†,‡] Dong Wu,*[†,‡] Shaochen Chen,[§,∥] and JiaRu Chu[†,‡]

[†]CAS Key Laboratory of Mechanical Behavior and Design of Materials and [‡]Department of Precision Machinery and Precision Instrumentation, University of Science and Technology of China, Hefei, Anhui 230027, China

[§]Department of Mechanical and Aerospace Engineering and [∥]Department of NanoEngineering, University of California, San Diego, La Jolla, California 92093, United States

Supporting Information

ABSTRACT: This article presents a new method for fabricating complex cross-sectional microtubes with a high aspect ratio at micro/nanoscale. The microtubes are directly written in a photoresist using a femtosecond pulsed laser combined with a spatial light modulator (SLM). A new method for generating a C-shaped Bessel beam by modifying the Bessel beams with a SLM is reported for the first time. Using this gap-ring-shaped light field, microtubes with special cross section (trefoil-shaped, clover-shaped, spiral, etc.) have been first achieved through two-photo polymerization rapidly. The microtube wall can reach about 800 nm and the diameter of the gap-ring structure is only a few micrometers. As a demonstration, artificial stomata were manufactured with the same size as actual plants stomata consisting of gap-ring microtubes. This artificial stomata can mimic the function of the real stomata with rapid opening and closing, demonstrating its ability to trap and release microparticles regulated by rinse solvent.

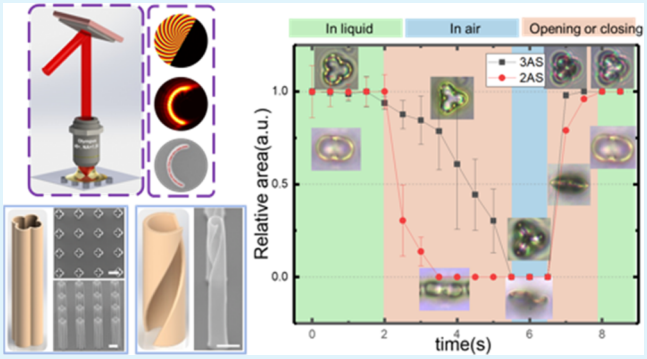

KEYWORDS: *femtosecond laser, Bessel beams, light phase modulation, complex-shaped microtubes, stomata*

1. INTRODUCTION

The micro/nano hollow-microtubes structures have attracted wide interest of material and chemical scientists because of their advanced functions in the development of new-generation devices and systems.[1,2] It can be used in special and important areas, for example, catalysis,[3] localized drug delivery,[4] neuroscience,[5] microsensors,[6] and microfluidic applications.[7] Many fabrication approaches have been utilized to create functional microtubes, including photolithography,[8] self-rolled-up driven by a stressed nanomembrane,[9] and direct laser writing (DLW).[10] In these methods, femtosecond direct laser writing (DLW) is a promising approach with great advantages such as high resolution, true-three-dimensional (3D) processing ability, and processing flexibility. Compared with the conventional photolithography, the microtubes fabricated by the femtosecond DLW are smaller and finer.[11] However, the fabrication of microstructures by the DLW technique needs a long time because the single-spot scanning method leads to low fabrication efficiency.

Recently, two-photo polymerization (TPP) using a femtosecond laser coupled with a spatial light modulation (SLM) has been developed for its fine resolution and high processing efficiency. In theory, the SLM can create an arbitrary light field by modulating the wave front of the laser beam. To improve the TTP efficiency, structured beams[12−15] modulated by SLM with different intensity distribution have been used to create functional structures. Among these structured lights, Bessel beams have their unique features such as nondiffraction, "self-healing", and possession of orbital angular momentum. Previously, our group has presented focused femtosecond laser Bessel beam generation technique for the rapid manufacture of microtube arrays.[16] The manufacturing time is reduced by 2 orders of magnitude compared with a conventional single-point scanning. However, owing to the circular intensity distribution of the Bessel beam, only the microtubes with a circular cross section can be fabricated, and these simplified microtubes cannot meet the increasing need of various applications such as biomimetic engineering and tissue

Received: July 5, 2018
Accepted: September 18, 2018
Published: September 18, 2018

DOI: 10.1021/acsami.8b11173
ACS Appl. Mater. Interfaces 2018, 10, 36369−36376

engineering. For example, stomata on the leaf surface has a pair of guard cells that forms a noncircular section. Compared with circular micropores, the noncircular ones are more easier to open and close to exchange gases between plant and its environment.[17] In tissue engineering, artificial thick tissues or organs can hardly be used in clinical application because they lack a hierarchical vascular network, which is typically responsible for sufficient nutrients and oxygen transport.[18] Until now, it is very difficult to fabricate biomimetic microvascular networks, and the rapid fabrication method of the microscopic branched hollow microtubes has not been resolved.

In this study, we demonstrate a simple and flexible method to generate a C-shaped Bessel beam by using local modulation of the Bessel beam's phase. The center angle and the diameter of the C-shaped light field can be modulated flexibly by controlling the shape of the local phase area and the hologram. Using this special beam, gap-ring-shaped microtubes and complex-patterned microstructure are fabricated by patterned light exposure. Compared to a single-point scanning method, this method increases the processing efficiency by 2 orders of magnitude. Besides, we design a new type of artificial stomata (AS) inspired by nature that consists of gap-ring microtubes that can open and close in seconds to release the trapped microparticles. The gap-ring-shaped light field and the hollow tubular structures have great potential in the field of drug delivery, cell capture and analysis, optical tweezers, and optical communication.

2. RESULTS AND DISCUSSION

2.1. Generation of C-Shaped Light Field and Fabrication of Gap-Ring Microstructure. The gap-ring structure is fabricated by focusing the C-shaped laser beam into a photoresist, and the fabrication setup is depicted in Figure 1a. The femtosecond laser is modulated by a hologram displayed on a reflective liquid-crystal SLM. After the modulation of SLM, a C-shaped laser beam is generated (inset in Figure 1b). At last, the modulated laser beam is focused by a 60× oil-immersion objective lens (Olympus, numerical aperture (NA) 1.35) for TPP, and the fabricated C-shaped structure is shown in Figure 1b, which agrees well with the intensity distribution.

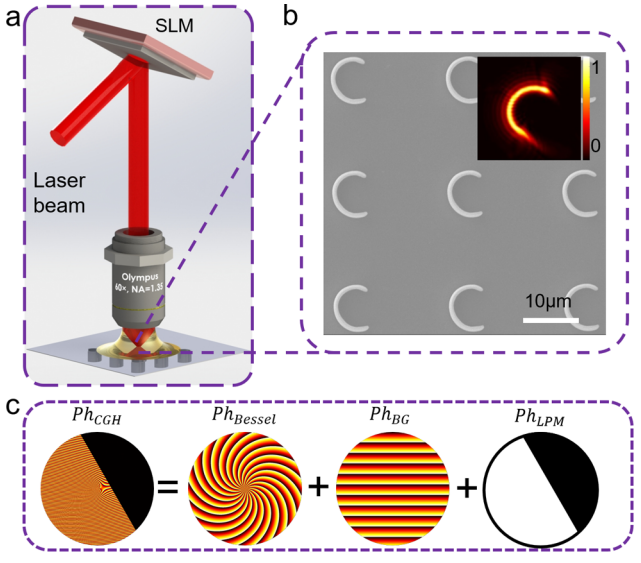

Figure 1. Method of creating gap-ring-shaped light field. (a) Femtosecond gap-ring-shaped beam is generated by phase modulation using a predesigned hologram loaded in the SLM. (b) The simulation of focused light field using Fresnel diffraction. (c) Illustration of the computer-generated hologram (CGH) with topological charge n = 20, axicon radius r_0 = 600 μm, blazed grating (BG) period Δ = 15 μm, and L = 200 pixels.

The computer-generated holograms (CGH) have three parts: Bessel beam phase (BBP), blazed grating (BG), and local phase modulation (LPM), as shown in Figure 1c. The BBP, composed of a spiral phase plate (SPP) and a axicon, is used to create a ring-shaped light field. The azimuthal phase of SPP is $n\varphi$, and the topological charge n is an integer that can be greater than zero and less than zero or equal to zero, representing the order of Bessel beam. If n is positive/negative, it means that the Bessel beam carries a positive/negative angular momentum. If n equals zero, it represents that the modulated beam is a zero-order Bessel beam. The phase distribution of axicon can be described as $2\pi r/r_0$, in which r_0 represents the axicon radius. Besides, the distribution of the BG phase can be written as $2\pi x/\Delta T$, in which ΔT is the blazed grating period. Thus, the phase of BBP and BG can be described as

$$\mathrm{Ph}_{\mathrm{Bessel}}(x, y) = \mathrm{mod}\left(n\varphi + \frac{2\pi r}{r_0} + \frac{2\pi x}{\Delta T}, 2\pi\right) \quad (1)$$

where $\mathrm{Ph}_{\mathrm{Bessel}}(x, y)$ is the phase distribution at the Cartesian coordinate, $\varphi = \arctan(y/x)$ represents the polar angle of the Bessel beam, and $r = \sqrt{x^2 + y^2}$ is the Bessel beam polar radius.

The shape of the local phase modulation area is the difference between the sector area and the triangle area composed of a chord and two radii (Figure S1, the Supporting Information); the black area means the phase distribution is zero, whereas the white area means the phase distribution is unchanged (Figure 1c). The phase of LPM can be written as two parts, phase 1 and phase 2. Phase 1 determines the radius of the LPM (R), whereas phase 2 identifies the distance from the center to the chord of the LPM (the length is L). Hence, the two phases can be described as

$$\mathrm{Ph}_{\mathrm{LPM1}}(x, y) = \begin{cases} 0 & \text{else} \\ 1 & k \le L \end{cases} \quad (2)$$

$$\mathrm{Ph}_{\mathrm{LPM2}}(x, y) = \begin{cases} 0 & \text{else} \\ 1 & r \le R \end{cases} \quad (3)$$

$$k = x \times \cos(\varphi) + y \times \cos(\varphi) \quad (4)$$

The phase of the LPM can be written as

$$\mathrm{Ph}_{\mathrm{LPM}} = \mathrm{Ph}_{\mathrm{LPM1}} \cap \mathrm{Ph}_{\mathrm{LPM2}} \quad (5)$$

Therefore, the synthetic phase distribution of the hologram can be described as

$$\mathrm{Ph}_{\mathrm{CGH}}(x, y) = \mathrm{Ph}_{\mathrm{Bessel}} \cap \mathrm{Ph}_{\mathrm{LPM}} \quad (6)$$

Due to the pixilation effect of the SLM, the BG phase is an important parameter to separate the zeroth order light from the other modulated laser beams.

2.2. Parameter Regulation of Gap-Ring Structure. The diameter and center angle of the gap-ring are essential in fabricating the required microstructures. The center angle is

DOI: 10.1021/acsami.8b11173
ACS Appl. Mater. Interfaces 2018, 10, 36369−36376

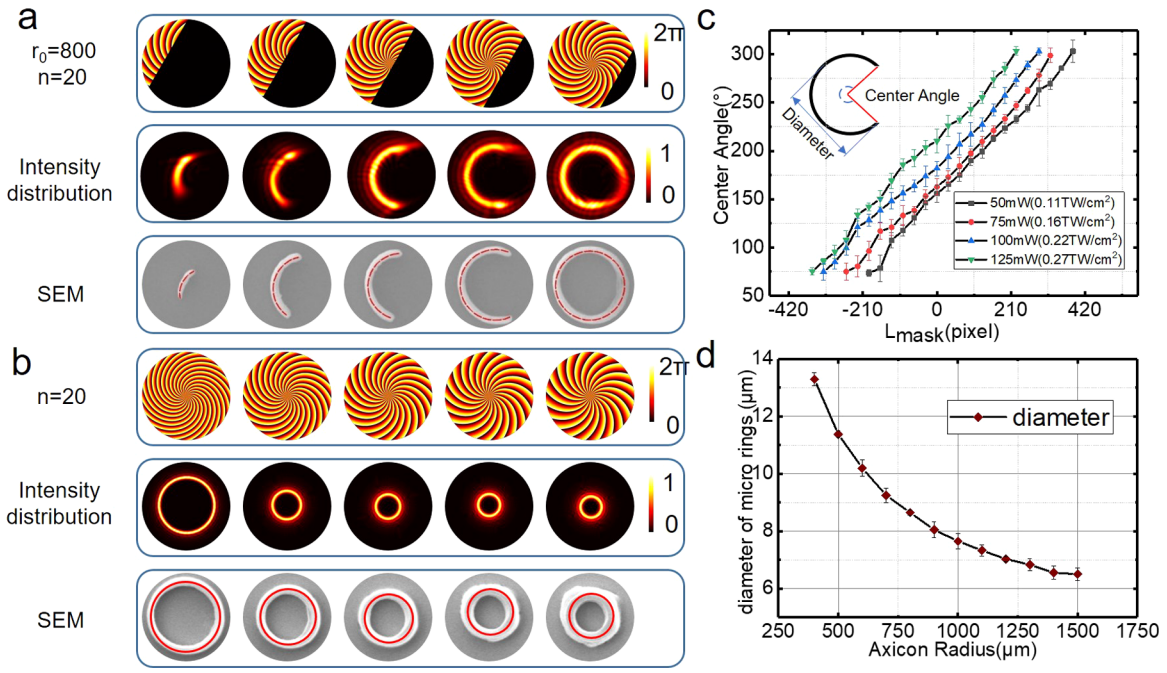

Figure 2. Parameter adjustment of gap-ring-shaped light field. (a) Adjustment of center angle: the first line is holograms with different L_{mask} and the same r_0 = 800 and n = 20 (the value of L_{mask} from left to right is −250, −100, 50, 200, and 350). The second row is the corresponding simulated light field calculated by Fresnel diffraction. The third line photos are SEMs of different gap-ring structures with different center angle. (b) Gap-ring structure diameter adjustment. The first row is holograms with different r_0 and the same n = 20 (the value of r_0 from left to right is 500, 700, 900, 1100, and 1300). The second row is the corresponding simulated light field calculated by Fresnel diffraction. The third row is the SEMs of the ring with different diameter. (c) The center angle of the gap-ring structure as a function of laser power and L_{mask}. Different laser power marked with different colors. (d) The diameter of the single-ring microstructures as a function of axicon radius.

controlled over the LPM, in which the area is reflected through the length of the hologram's center to the chord. The control of Bessel beam shaped is achieved by controlling the shape of LPM area. To clarify the consistency of the simulation and the experimental results, the Fresnel diffraction theory was adopted to simulate the C-shaped light fields generated by the CGHs. Figure 2a demonstrates a series of simulated results and reveals the relationship between L and the center angle. The first row was a series of CGHs for generating the C-shaped light, whereas the simulated results was illustrated in the second row of Figure 2a. All the CGHs have the same r_0 = 800 and n = 20 but different L, −250, −100, 50, 20, and 350 (unit: pixel value), respectively. According to the simulation, it can be concluded that the central angle increases with increasing L, so the center angle of the gap-ring can be adjusted by changing the L. In addition, a series CGHs with continuously changing L were used for exposure processing, and the center angle of the gap-rings were measured by scanning electron microscopy (SEM) images in Figure 2b. The measured results showed that the center angle of the gap-ring increased with L, which agreed well with the theoretical simulation. Additionally, a good linear relationship between the center angle and L was observed, indicating that the center angle of the gap-ring could be coordinated by changing L. The third row of Figure 2a is a series of SEM images with the center angle of the gap-rings structure increasing from 75 to 300°. The red dotted lines indicated the geometry of the gap-rings. In addition, the gap-ring structure had good processing quality that matched the theoretical geometry. Because the intensity distribution of the C-shaped light field was uniform, it was suitable for fabricating the gap-ring microtubes. Besides, laser polarization has little effect on the processing results, which is shown in Figure S6.

Notably, the C-shaped Bessel beam is an asymmetric beam. Currently, the methods to generate an asymmetric Bessel beam mainly depends on the asymmetric distribution and superposition of the Bessel beam topology charges.[19−21] In contrast, this method relies on LPM, is simple, and produces a C-Bessel beam with a uniform light distribution. Moreover, the gap-ring size and the center angle can be regulated flexibly. This C-shaped Bessel beam may have remarkable potential applications in the field of optical communications and tweezers.

Because TPP is a nonlinear polymerization process,[22] the laser power has great impact on the exposure of the gap-ring structure. A larger fabrication power will polymerize a greater area, resulting in a bigger center angle. As revealed in Figure 2b, four groups of different laser power (50, 75, 100, and 125 mW) were used to process the same CGHs. Besides, for better explaining the mechanism of the laser−matter interaction, the light intensity should be considered. As the femtosecond laser we used has a central wavelength λ = 800 nm with a pulse repetition rate f = 80 MHz and pulse width τ = 75 fs, the 50 mW of the average power equals to 0.108 TW/cm^2 of laser intensity.[23−25] It can be observed that the curves shifted to the left with an increasing laser power. When the measurement error is taken into account, the curves shift can be considered linear. Besides, the average power also affects the line width of the micro-gap-ring structure.[26,27] As shown in Figure S5, when the power is 60 mW, the thickness of the microtubes is about 700 nm. As the power increase to 190 mW, the thickness of the microtubes increases to 3.7 μm.

The regulation of the gap-ring's diameter can be achieved through changing r_0 and n, here mainly r_0. The SEM images

DOI: 10.1021/acsami.8b11173
ACS Appl. Mater. Interfaces 2018, 10, 36369−36376

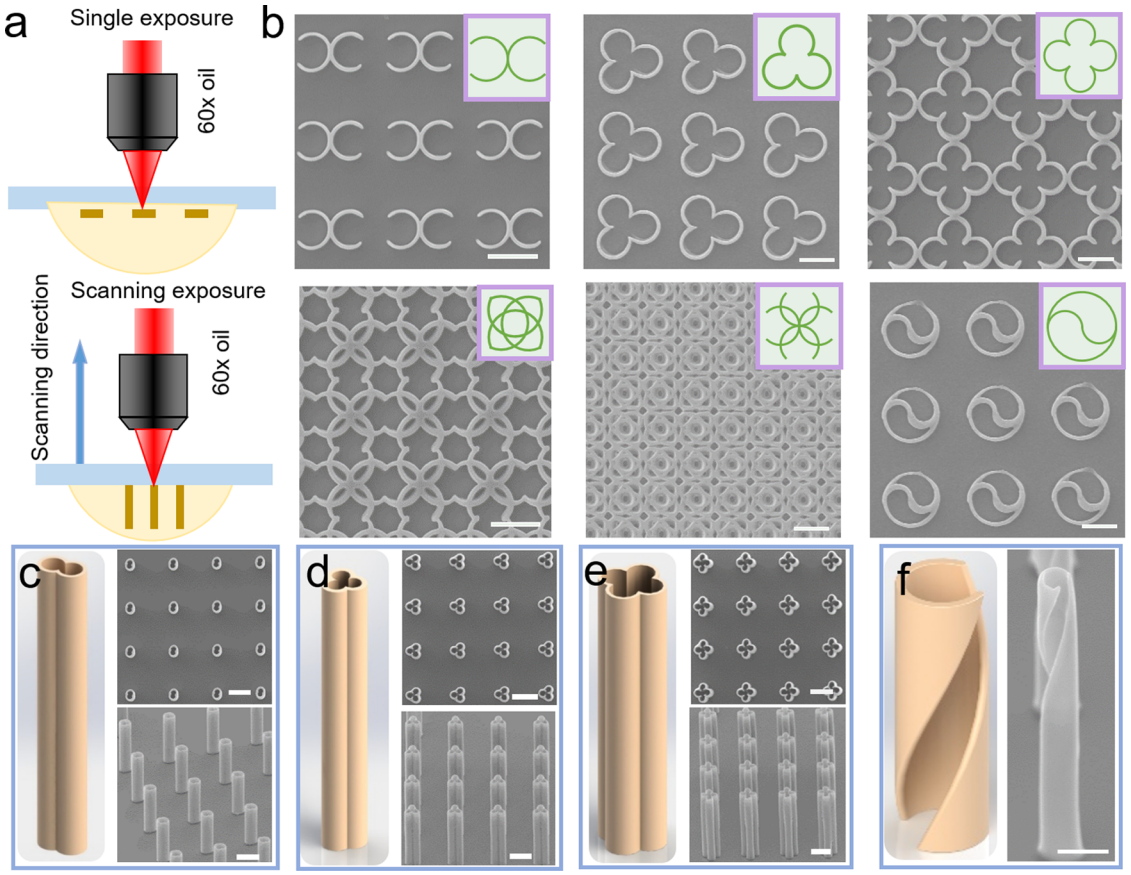

Figure 3. Process of patterned structure and complex microtubes. (a) Schematic illustration of two processing methods. In single exposure, the shaped laser beam stays in a position for a certain amount of time. In scanning exposure, the 3D stage moves along the *z*-direction during the laser beam exposure. (b) The SEM of complex-patterned structure from single exposure. The shapes are X-shaped, trefoil-shaped, clover-shaped, flower-shaped, rose-shaped, and Tai Chi-shaped (scale bar: 10 μm). (c, e) Complex microtube arrays with special shaped cross section are produced by scanning exposure processing, a challenge for other fabrication methods. (f) The SEM of microtube with spiral open cross. The scale bar of (c)−(f) is 20 μm.

and the simulated results of CGHs with different r_0 are shown in Figure 2c. The r_0 of five CGHs in Figure 2c were 500, 700, 900, 1100, and 1300, respectively. When r_0 increased from 300 to 1100, the diameter of the gap-ring decreased from 9.5 to 3.5 μm at the average laser power of 80 mW. Besides, the gap-ring's diameter could be adjusted by changing the objective lens. For example, micro rings structure with a diameter of 40 μm can be obtained by using a 20× objective lens, which is much larger than a micro ring structure fabricated with a 60× objective.

2.3. Rapid Processing of Patterned Structure and Complex-Shaped Microtubes. Our gap-ring-shaped light field can be employed to process not only a simple notched ring structure but also complicated patterned structure and tubes by controlling the 3D nanotranslation stage to determine the location and height of the gap-rings. As shown in Figure 3a, two processing strategies were used: single exposure and scanning exposure. In single exposure, the 3D stage remains immovable at a certain position for a certain exposure time, whereas in the scanning exposure, the 3D stage moves along the *z*-direction for a certain exposure time.

First, the gap-ring-shaped light field was designed and generated by imprinting the predesigned holograms on the SLM. Then, with the aid of computer-programming control, the 3D stage was moved in the predesigned path. As a result, different gap-rings were exposed at different positions and patterned structures were obtained. Finally, the processed photoresist was soaked in *n*-propanol for 1 h, and the unprocessed area was removed. Figure 3b shows the patterned structure such as X-shaped, clover-shaped, flower-shaped, and Tai Chi-shaped by single exposure. The processing time of each single gap-ring structure is 500 ms, which can be reduced to 100 ms or even 10 ms by increasing the power of the laser beam. This surface-patterned technology with a high speed has broad prospects in fields such as micro-optics, biomedical applications, microfluidic, and so on.[28]

Single-gap-ring microtubes were obtained by scanning exposure and complex cross-sectional microtubes were fabricated by assembling gap-ring microtubes. In this way, microtubes with complex cross shapes were obtained as shown in Figure 3c−e. Remarkably, if CGHs with continuously different phase were projected on the SLM while the 3D stage was moving, microtubes with a spiral open cross could be obtained (Figure 3f), and the spiral opening structure of microtubes is difficult to manufacture rapidly by other micro/nanoprocessing methods.

It should be pointed out that the height of the microtubes can be up to the oil-immersion lens working distance because the microtubes are manufactured by moving the sample adhered to the 3D stage along the z-direction. Therefore, this method could yield structure with an aspect ratio of 20 or even more. Furthermore, it is important to highlight that these

DOI: 10.1021/acsami.8b11173
ACS Appl. Mater. Interfaces 2018, 10, 36369−36376

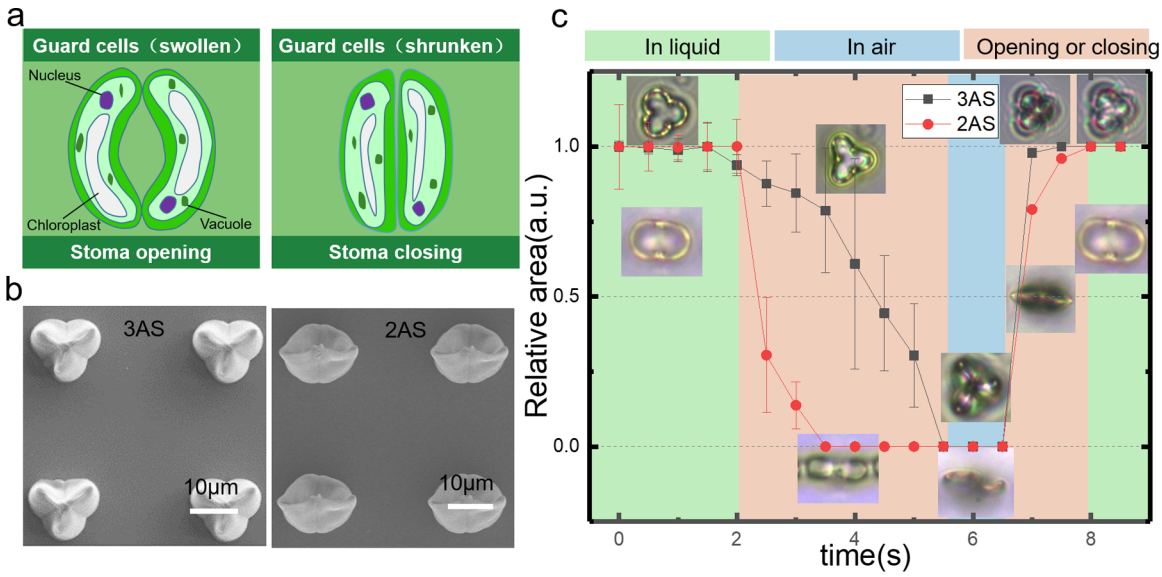

Figure 4. Fabrication of artificial stomata and its closing and opening. (a) The stomata consists of a pair of guard cells. The stomata is open when guard cells swell up and is closed when the guard cells shrink down. (b) Two different types of artificial stomata: 2AS and 3AS. (c) The open and closing process of AS. The abscissa is the time, the ordinate is the relative area, and three colors represent the three states of AS: green areas indicate that the structure is in solution, brown areas indicate that the solution is opening or closing, and blue areas indicate that the structure is in the air.

complex microtubes are difficult to make through other fabrication methods. In addition, the manufacturing time for a two-gap-ring microtubes (150 μm high) at the scanning speed of 40 μm/s along the z-direction is less than 10 s, which is much shorter than that of single-point scanning (ten of minutes). The wall thickness of the gap-ring microtubes is only about 800 nm through this method (Figure S2b,c), and the diameter and gap sizes can be regulated by design. Compared with the existing methods such as photolithography and self-roll-up, this method, based on SLM-aided TPP, can quickly process gap-ring-shaped microtubes with a high aspect ratio and controllable gap. Hence, this processing method has the ability to fabricate high-aspect-ratio microtubes with complex cross shapes efficiently and reliably. It has great potential for applications in bionics, medicine, microfluidics, etc.

2.4. Fabrication of Biomimetic Plant Stomata. Stomates are micro-sized pores distributed on the surface of the leaves, are important part of plant leaves, and can regulate water flow and gases like CO_2 according to the plant's needs and water availability.[29,30] As illustrated in Figure 4a, a pair of guard cells control the opening and closing of the stomata, which works like multisensory turgor-operative valves and can exchange gases between the environment and the plant. Lots of biomimetic technologies have been developed based on the function of stomata, such as evaporative pumps, artificial leaves,[31,32] and stimuli-responsive hydrogel.[33] Due to the ability of stomata to allow the uptake of carbon dioxide and limit the water loss, much work has focused on the fabrication of artificial stomata. For example, the artificial stomata consisting of two different hydrogels, which swell differently in the same solution, was developed by Gargava A et al.[34] In addition, a temperature-responsive hydrogel through patterned photopolymerization was used to realize a stomata-inspired membrane.[33] Nevertheless, there are still several issues in the artificial stomata that deserve further discussion: (1) the size of the minimum artificial stomata is about 500 μm, 10 times that of the real stomata; (2) the response speed of the stomata opening and closing is too slow; and (3) the artificial stomata cannot achieve 100% closure and single completely closed artificial stomata cannot be guaranteed.

The material used for fabricating the AS should be deformable for realizing the opening and closing movements. It was demonstrated in a number of studies that SZ2080 can deform after soaking in a polar solution or move by capillary action.[13,35−37] Generally, the deformation is widely regarded as an irreversible process that leaves a permanent impact on the size and shape of the dry structure. However, it is helpful to note that reversible size modifications may also be expected to occur before drying when the samples are immersed in the developer solvent.

Here, with the advantages of SZ2080's reversible deformation, an innovative stomata-inspired structure was designed for the first time. Fabricated with the same size as that of the real stomata, it can open and close in a few seconds. Moreover, because the AS structure is hollow, it could trap gas and microparticles and release them in a solution.

The stomata on plant leaves are bordered by a pair of specialized parenchyma cells known as the guard cells (Figure 4a); hence, two or three gap-ring-shaped microtubes were fabricated to form an artificial stomata. The diameters of the gap-ring-shaped microtubes were 12 and 10 μm for a two-gap-ring (2AS) and three-gap-ring AS (3AS) with the same height (20 μm), respectively (Figure 4b). Owing to the requirements of AS's structural rigidity, the laser power was crucial during the fabrication of AS. If the laser power is too high, the AS will not close with the evaporation of the solution. On the other hand, if the laser power is too low, the AS will collapse during the solution evaporation due to the lack of rigidity. Therefore, an optimal laser power was required to fabricate the AS. After optimization, we found a laser power of 40 mW and a scanning speed of 20 μm/s for scanning exposure could yield the required AS. To improve the success rate of processing, a double-exposure strategy was also adopted to reinforce the stiffness of the AS. After finishing the AS, the same gap-ring

DOI: 10.1021/acsami.8b11173
ACS Appl. Mater. Interfaces 2018, 10, 36369−36376

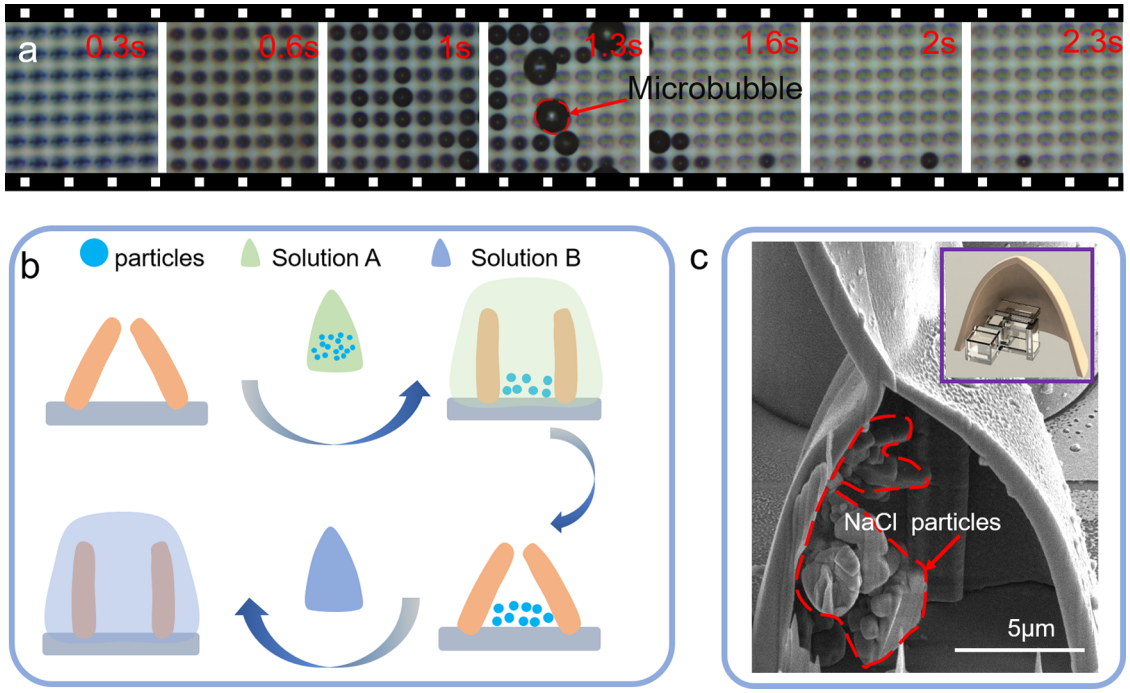

Figure 5. Release of microbubbles and the trapping and release of microparticles. (a) Optical photos of microbubbles released by artificial stomata at different times. (b) Schematic diagram of trapping and release of microparticles. (c) Image of artificial stomata cut by focused ion beam (FIB), the illustration in the upper right shows the position of microsalt particles in the AS.

light field was used to expose the bottom of the AS again to increase the stiffness of its bottom through the second exposure. In this way, the stiffness at the top is lower than that at the bottom, enabling reversible deformation of the AS and good adhesion of the AS to the substrate.

In nature, the opening and closing of the stomata on the leaves are regulated by the expansion and contraction of the guard cells. When the guard cells of the stomata are swollen with water, the cells separate, causing the stomata to open and allowing water or gas to pass. Conversely, when the guard cells are dehydrated, the guard cells move toward each other, causing the stomata to close and block the moisture through transpiration. Similarly, our artificial stomata's opening and closing were regulated by the solvent. The AS remains open in the solvent but closes under capillary force (FC) when the solvent evaporates.

Theoretically, the opening and closing of the AS were consequence of the competition between the capillary force (FC) caused by the solution evaporation and the standing force (FS) caused by the rigidity of the microstructure. As show in Figure S4a,b, when the artificial stomata is about to close due to the evaporation of the solution, a meniscus arises in the microstructure and causes an asymmetric capillary along the tangential direction of the solution surface, which is determined by the contact angle. As the FC increases to a certain value that is enough to overcome the FS, the microstomata begins to close. After closing, the top parts of the AS contact with each other, causing the van der Waals force (FV), which continues to overcome the FS and keep the AS closed (Figure S4c,d). When the AS is immersed in the solution, the liquid molecules enter into the gaps of the top part of the AS, causing the FV to decrease and resulting in the open structure.

Another interesting finding was that the opening and closing of the AS were very rapid and only took a few seconds because the FS, FC, and FV can be quickly produced and disappeared. Figure 4c shows the relative area variation in a period of AS opening and closing. The relative area was the total area divided by the open area of the AS, which indicates the degree of the stomata's opening. The value of 100% implies complete opening, whereas 0% implies complete closure. In the first 2 s, the AS was immersed in the liquid and kept open. Followed by the evaporation of *n*-propyl alcohol, the 2AS and 3AS close rapidly in 1.5 and 3.5 s, respectively. When the AS was exposed to air, the AS kept closed due to FV between the top parts of the AS. Finally, the AS opened again when immersed in the liquid, and the opening process only took 1 s. The videos of the artificial stomata opening and closing are shown in the Supporting Information (Videos S1 and S2).

2.5. Trapping and Releasing Microparticles by Artificial Stomata. It is well known that stomatal movement is important for plants. With the opening and closing of the stomata, gas, water, and nutrients are exchanged with the external environment. Hence, it is important for the the artificial stomata to achieve the same function such as controlling the entry and exit of gas/nutrients.

First, due to the close contact of the edges of the AS, a good seal results in the AS being able to store gas and release them in liquid, like a valve. When the AS was closed, the top of the AS was in close contact and the bottom of the AS did not deform, causing a gap in the AS. When the closed AS was surrounded by a liquid environment, the FV disappeared rapidly and the AS opened in a second, causing the liquid to fill the hollow space quickly and expel the gas. As a result, microbubbles were formed (Video S3, the Supporting Information). As can be seen in Figure 5a, each AS generated a microbubble whose diameter was about 10 μm at the beginning and increased to about 30 μm with the merging of the microbubbles. This interesting phenomenon verified that

DOI: 10.1021/acsami.8b11173
ACS Appl. Mater. Interfaces 2018, 10, 36369−36376

the structure was hollow, which could be useful in cell trapping and drug delivery applications.

Second, the AS could serve as a microscale trap−release system to trap, transfer, and release the nutrients such as sugar and salt (Figure 5b). First, we dropped a mixture of microparticles and solvent A, in which the microparticles are insoluble in solvent A, onto the AS to open it. As the microparticles precipitated, they fell into the AS and got trapped. Next, the AS closed as the solvent A evaporated and thus trapped the microparticles permanently and reliably. Finally, solvent B dissolved the microparticles in the AS, causing it to open and release the trapped particles.

As a proof-of-concept demonstration, we use sodium chloride (NaCl) particles, which are soluble in water (solvent B) but almost insoluble in ethanol (solvent A). Figure S3b shows the optical pictures corresponding to Figure 5b, and the trapped NaCl microparticles are marked by yellow circle. To verify that there were trapped particles in the artificial stomata, focused ion beam (FIB) was used to cut the structure (Figure 5c). The FIB photos showed that the trapped particles were present within the AS, demonstrating that the method of trapping and releasing the particles in different solutions is feasible and effective.

3. CONCLUSIONS

In this work, a gap-ring-shaped light field was generated by using a new method to modify the hologram of the Bessel beam. The center angle and the diameter of the gap-ring were controlled by adjusting the parameters of the hologram and changing the objective lens. Using this special light field, patterned structure and microtubes with complex cross-sectional shape were fabricated quickly and efficiently. Besides, inspired by the stomata of a plant, the stiffness of microtubes was reduced and microtubes with controllable opening and closing are obtained. The artificial stomata not only open and close within seconds but also store gas and perform trapping and release of microparticles like a real stomata in nature. These artificial stomates, which control the entry and exit of materials, have great potential in applications such as drug delivery, cell capture, and analysis. Beside fabrication, the gap-ring-shaped light field could be useful in the field of optical tweezers and optical communication.

4. EXPERIMENTAL SECTION

1. The preparation of sample: the photoresist we used is SZ2080, which was mixed with 1 wt % 4,4-bis(diethylamino)-benzophenone as photoinitiator (IESL-FORTH). Fifteen microliters of SZ2080 was added dropwise to the glass slide, which was placed on a hot plate and heated at 100 °C for 1 h.
2. The manufacture of microstructure: the femtosecond laser is a mode-locked Ti:sapphire ultrafast oscillator (Chameleon Vision-S, from Coherent Inc., Santa Clara, CA). The central wavelength of the laser is 800 nm, the pulse width is 75 fs, and the repletion rate is 80 MHz. After the expansion, the laser beam is projected onto the SLM, which is a reflective liquid-crystal SLM (Holoeye Photonics AG, Berlin, Germany, Pluto NiR-2). The modulated laser beam is focused by an oil-immersed objective lens (60×, NA 1.35, Olympus). The sample is put on the 3D nanostage (E545, from Physik Instrumente (PI) GmbH & Co. KG, Germany). After fabrication by femtosecond laser, the samples are soaked in *n*-propanol for 1 h to remove unprocessed areas.
3. The sample characterization and imaging: the optical images are taken by microscopy (Leica, DMI 3000B) and the SEM images are taken by electron scanning electron microscope (ZEISS EVO18) with an accelerating voltage 10 keV.

ASSOCIATED CONTENT

Supporting Information

The Supporting Information is available free of charge on the ACS Publications website at DOI: 10.1021/acsami.8b11173.

Parameters of LPM; trapping and releasing micro particles; specific explanation of capillary force, standing force and van der Waal's force (PDF)

Opening and closing of artificial stomata consisting of 2-gap-ring (2AS) and 3-gap-ring microtubes (3AS), respectively (AVI) (AVI)

Artificial stomata generates microbubbles when immersed in liquids (AVI)

AUTHOR INFORMATION

Corresponding Authors

*E-mail: jwl@ustc.edu.cn (J.L.).
*E-mail: dongwu@ustc.edu.cn (D.W.).

ORCID

Liang Yang: 0000-0001-6103-6451
Jiawen Li: 0000-0003-3950-6212
Yanlei Hu: 0000-0003-1964-0043
Dong Wu: 0000-0003-0623-1515
JiaRu Chu: 0000-0001-6472-8103

Notes

The authors declare no competing financial interest.

ACKNOWLEDGMENTS

This work was supported by the National Science Foundation of China (Nos. 51675503, 61475149, 51875544, 61805230, 51805508, and 51805509), the National Key R&D Program of China (2018YFB1105400), the Fundamental Research Funds for the Central Universities (WK 2090090012, WK2480000002, and WK2090090021), and Youth Innovation Promotion Association CAS (2017495). This work was partially carried out at the USTC Center for Micro and Nanoscale Research and Fabrication. We acknowledge the Experimental Center of Engineering and Material Sciences, USTC.

REFERENCES

(1) Liu, W.; Zhang, L.; Cao, L.-X.; Su, G.; Wang, Y.-G. Glass Fibers Templated Preparation of TiO2 Microtubes Assembled from Nano/Micro Hierarchical TiO2 Crystals. *J. Alloys Compd.* **2011**, *509*, 3419−3424.

(2) Stankevicius, E.; Gertus, T.; Rutkauskas, M.; Gedvilas, M.; Raciukaitis, G.; Gadonas, R.; Smilgevicius, V.; Malinauskas, M. Fabrication of Micro-tube Arrays in Photopolymer SZ2080 by Using Three Different Methods of a Direct Laser Polymerization Technique. *J. Micromech. Microeng.* **2012**, *22*, No. 065022.

(3) Gao, W.; Sattayasamitsathit, S.; Orozco, J.; Wang, J. Highly Efficient Catalytic Microengines: Template Electrosynthesis of Polyaniline/Platinum Microtubes. *J. Am. Chem. Soc.* **2011**, *133*, 11862−11864.

(4) Takei, K.; Kawashima, T.; Kawano, T.; Kaneko, H.; Sawada, K.; Ishida, M. Out-of-plane Microtube Arrays for Drug Delivery—Liquid Flow Properties and an Application to the Nerve Block Test. *Biomed. Microdevices* **2009**, *11*, 539−545.

(5) Froeter, P.; Huang, Y.; Cangellaris, O. V.; Huang, W.; Dent, E. W.; Gillette, M. U.; Williams, J. C.; Li, X. Toward Intelligent Synthetic Neural Circuits: Directing and Accelerating Neuron Cell Growth by

Self-rolled-up Silicon Nitride Microtube array. *ACS Nano* **2014**, *8*, 11108−11117.
(6) Smith, E. J.; Schulze, S.; Kiravittaya, S.; Mei, Y.; Sanchez, S.; Schmidt, O. G. Lab-in-a-tube: Detection of Individual Mouse Cells for Analysis in Flexible Split-wall Microtube Resonator Sensors. *Nano Lett.* **2011**, *11*, 4037−4042.
(7) Wu, D.; Niu, L. G.; Wu, S. Z.; Xu, J.; Midorikawa, K.; Sugioka, K. Ship-in-a-bottle Femtosecond Laser Integration of Optofluidic Microlens Arrays with Center-pass Units Enabling Coupling-free Parallel Cell Counting with a 100% Success Rate. *Lab Chip* **2015**, *15*, 1515−1523.
(8) Sánchez, S. Lab-in-a-tube Systems as Ultra-compact Devices. *Lab Chip* **2015**, *15*, 610−613.
(9) Choe, Y.; Kim, J. W.; Shung, K. K.; Kim, E. S. Microparticle Trapping in an Ultrasonic Bessel Beam. *Appl. Phys. Lett.* **2011**, *99*, No. 233704.
(10) Wang, H.; Zhang, Y. L.; Zhu, R.; Chen, D. L.; Jin, G. X.; Sun, H. B. Femtosecond Laser Direct Writing of Ion Exchangeable Multifunctional Microstructures. *Opt. Lett.* **2018**, *43*, 1139−1142.
(11) Zhang, Y.-L.; Chen, Q.-D.; Xia, H.; Sun, H.-B. Designable 3D Nanofabrication by Femtosecond Laser Direct Writing. *Nano Today* **2010**, *5*, 435−448.
(12) Ni, J.; Wang, C.; Zhang, C.; Hu, Y.; Yang, L.; Lao, Z.; Xu, B.; Li, J.; Wu, D.; Chu, J. Three-dimensional Chiral Microstructures Fabricated by Structured Optical Vortices in Isotropic Material. *Light: Sci. Appl.* **2017**, *6*, No. e17011.
(13) Ni, J.; Wang, Z.; Li, Z.; Lao, Z.; Hu, Y.; Ji, S.; Xu, B.; Zhang, C.; Li, J.; Wu, D.; Chu, J. Multifurcate Assembly of Slanted Micropillars Fabricated by Superposition of Optical Vortices and Application in High-Efficiency Trapping Microparticles. *Adv. Funct. Mater.* **2017**, *27*, No. 1701939.
(14) Yang, L.; Qian, D.; Xin, C.; Hu, Z.; Ji, S.; Wu, D.; Hu, Y.; Li, J.; Huang, W.; Chu, J. Two-photon Polymerization of Microstructures by a Non-diffraction Multifoci Pattern Generated from a Superposed Bessel Beam. *Opt. Lett.* **2017**, *42*, 743−746.
(15) Cai, Z.; Liu, Y.; Hu, Y.; Zhang, C.; Xu, J.; Ji, S.; Ni, J.; Lao, Z.; Li, J.; Zhao, Y.; Wu, D.; Chu, J. Generation of Colorful Airy Beams and Airy Imaging of Letters via Two-photon Processed Cubic Phase Plates. *Opt. Lett.* **2018**, *43*, 1151−1154.
(16) Yang, L.; Ji, S.; Xie, K.; Du, W.; Liu, B.; Hu, Y.; Li, J.; Zhao, G.; Wu, D.; Huang, W.; Liu, S.; Jiang, H.; Chu, J. High Efficiency Fabrication of Complex Microtube Arrays by Scanning Focused Femtosecond Laser Bessel Beam for Trapping/Releasing Biological Cells. *Opt. Express* **2017**, *25*, 8144−8157.
(17) Park, Y.; Gutierrez, M. P.; Lee, L. P. Reversible Self-Actuated Thermo-Responsive Pore Membrane. *Sci. Rep.* **2016**, *6*, No. 39402.
(18) Paulsen, S. J.; Miller, J. S. Tissue Vascularization Through 3D Printing: Will Technology Bring Us Flow? *Dev. Dyn.* **2015**, *244*, 629−640.
(19) Gong, L.; Qiu, X. Z.; Ren, Y. X.; Zhu, H. Q.; Liu, W. W.; Zhou, J. H.; Zhong, M. C.; Chu, X. X.; Li, Y. M. Observation of the Asymmetric Bessel Beams with Arbitrary Orientation Using a Digital Micromirror Device. *Opt. Express* **2014**, *22*, 26763−26776.
(20) Kotlyar, V. V.; Kovalev, A. A.; Skidanov, R. V.; Soifer, V. A. Asymmetric Bessel-Gauss Beams. *J. Opt. Soc. Am. A* **2014**, *31*, 1977−1983.
(21) Kotlyar, V. V.; Kovalev, A. A.; Soifer, V. A. Asymmetric Bessel Modes. *Opt. Lett.* **2014**, *39*, 2395−2398.
(22) Raimondi, M. T.; Eaton, S. M.; Nava, M. M.; Laganà, M.; Cerullo, G.; Osellame, R. Two-photon Laser Polymerization: from Fundamentals to Biomedical Application in Tissue Engineering and Regenerative Medicine. *J. Appl. Biomater. Funct. Mater.* **2012**, *10*, 55−65.
(23) Jonušauskas, L.; Juodkazis, S.; Malinauskas, M. Optical 3D Printing: Bridging the Gaps in the Mesoscale. *J. Opt.* **2018**, *20*, No. 053001.
(24) Jonušauskas, L.; Gailevicius, D.; Mikoliunaite, L.; Sakalauskas, D.; Sakirzanovas, S.; Juodkazis, S.; Malinauskas, M. Optically Clear and Resilient Free-Form micro-Optics 3D-Printed via Ultrafast Laser Lithography. *Materials* **2017**, *10*, No. 12.
(25) Rekštytė, S.; Jonavičius, T.; Gailevičius, D.; Malinauskas, M.; Mizeikis, V.; Gamaly, E. G.; Juodkazis, S. Nanoscale Precision of 3D Polymerization via Polarization Control. *Adv. Opt. Mater.* **2016**, *4*, 1209−1214.
(26) Malinauskas, M.; Farsari, M.; Piskarskas, A.; Juodkazis, S. Ultrafast Laser Nanostructuring of Photopolymers: A Decade of Advances. *Phys. Rep.* **2013**, *533*, 1−31.
(27) Malinauskas, M.; Zukauskas, A.; Bickauskaite, G.; Gadonas, R.; Juodkazis, S. Mechanisms of Three-dimensional Structuring of Photopolymers by Tightly Focussed Femtosecond Laser Pulses. *Opt. Express* **2010**, *18*, 10209−10221.
(28) Malinauskas, M.; Žukauskas, A.; Hasegawa, S.; Hayasaki, Y.; Mizeikis, V.; Buividas, R.; Juodkazis, S. Ultrafast Laser Processing of Materials: from Science to Industry. *Light: Sci. Appl.* **2016**, *5*, No. e16133.
(29) Lange, O. L.; Losch, R.; Schulze, E. D.; Kappen, L. Responses of Stomata to Changes in Humidity. *Planta* **1971**, *100*, 76−86.
(30) Mauseth, J. D. *Botany: An Introduction to Plant Biology*; Jones & Bartlett Publishers, 2011.
(31) Wheeler, T. D.; Stroock, A. D. The Transpiration of Water at Negative Pressures in a Synthetic tree. *Nature* **2008**, *455*, 208−212.
(32) Jingmin, L.; Chong, L.; Zheng, X.; Kaiping, Z.; Xue, K.; Liding, W. A Microfluidic Pump/Valve Inspired by Xylem Embolism and Transpiration in Plants. *PLoS One* **2012**, *7*, No. e50320.
(33) Kim, H.; Lee, S. J. Stomata-Inspired Membrane Produced Through Photopolymerization Patterning. *Adv. Funct. Mater.* **2015**, *25*, 4496−4505.
(34) Gargava, A.; Arya, C.; Raghavan, S. R. Smart Hydrogel-Based Valves Inspired by the Stomata in Plants. *ACS Appl. Mater. Interfaces* **2016**, *8*, 18430−18438.
(35) Hu, Y.; Lao, Z.; Cumming, B. P.; Wu, D.; Li, J.; Liang, H.; Chu, J.; Huang, W.; Gu, M. Laser Printing Hierarchical Structures with the Aid of Controlled Capillary-driven Self-assembly. *Proc. Natl. Acad. Sci. U.S.A.* **2015**, *112*, 6876−6881.
(36) Lao, Z. X.; Hu, Y. L.; Pan, D.; Wang, R. Y.; Zhang, C. C.; Ni, J. C.; Xu, B.; Li, J. W.; Wu, D.; Chu, J. R. Self-Sealed Bionic Long Microchannels with Thin Walls and Designable Nanoholes Prepared by Line-Contact Capillary-Force Assembly. *Small* **2017**, *13*, No. 1603957.
(37) Rekštytė, S.; Paipulas, D.; Malinauskas, M.; Mizeikis, V. Microactuation and Sensing Using Reversible Deformations of Laser-written Polymeric Structures. *Nanotechnology* **2017**, *28*, No. 124001.

DOI: 10.1021/acsami.8b11173
ACS Appl. Mater. Interfaces 2018, 10, 36369−36376